DETERMINATION OF ELECTRON DENSITY IN THE

JOVIAN MAGNETOSPHERE FROM

GALILEO PLASMA WAVE DATA

by

Benjamin H. Richards

A thesis submitted in partial fulfillment
of the requirements for the Master of
Science degree in Physics
in the Graduate College of
The University of Iowa

May 2006

Thesis Supervisor: Professor Donald A. Gurnett

Graduate College
The University of Iowa
Iowa City, Iowa

CERTIFICATE OF APPROVAL

_____

. MASTER'S THESIS

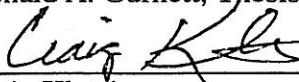_____

This is to certify that the Master's thesis of

Benjamin H. Richards

has been approved by the Examining Committee for the
thesis requirement for the Master of Science degree in
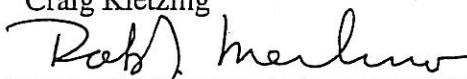Physics at the May 2006 graduation.

Thesis committee: _____
Donald A. Gurnett, Thesis supervisor

_____
Craig Kletzing

_____
Robert Merlino

To the memory of Helen Marjorie Richards
1923 – 2005

ACKNOWLEDGMENTS

service, I am extremely grateful. My degree would not have been possible without her efforts on my behalf. Another is Rich Huff who initially worked with me on Galileo data processing and has been a friend since. Both he and his wife Jolene Pickett have endured my sense of humor, and for such, I apologize. To my other friends I offer my thanks for their time, understanding, support, and couch: Aaron Breneman, Brent and Lindsey Canham, Richard and Becky Dafoe, Juan Diaz, Tim Flanagan, Tucker Friesmuth, Brandy Fuller, Sarah Iverson, Jason and Amanda Slattery, Chris Sloane, Dan and Veronica Smith, Lifi Somantri, Derek and Suzanne Thuecks, Brian Yulga, and Lindsey Waibel. To those who have accidentally been left off, I apologize.

My family, of course, has their own place in my life. To my parents, Danny and Nancy; brother, Nick; grandparents; and Jason Parker, who might as well be a brother, thank you for your continuing confidence and trust.

ABSTRACT

An analysis of the electron density in the Jovian magnetosphere is presented from data gathered by the Galileo spacecraft's plasma wave instrument. Two techniques are employed. The first uses the low frequency cutoff of trapped continuum radiation at the local electron plasma frequency, $f_p = 8980\sqrt{n_e}\,Hz$, where n_e is the electron density in cm^{-3}. The second uses a narrow band emission at the upper hybrid resonance frequency, $f_{uh} = \sqrt{f_p^2 + f_c^2}\,Hz$, where $f_c = 28B\,Hz$ defines the electron cyclotron frequency with B in nanoTesla, and is primarily used inside approximately 20 R$_J$, where the first method fails. The data analyzed covers the time period between December 1995 and November 2002. The radial distances covered range from approximately 4 R$_J$, near the inner edge of the cold torus, to approximately 150 R$_J$. Local times extend from approximately 2000 hours in the local evening, through local midnight, to 0400 hours local morning. Electron densities vary from approximately 4×10^3 cm^{-3}, in the densest regions of the Io torus, to 10^{-2} cm^{-3} in the distant magnetotail. The radial electron density profile has a distinct break at approximately 24 R$_J$ and varies as approximately $(1/r)^{7.5 \pm 0.4}$ from 6 to 24 R$_J$ and as $(1/r)^{2.08 \pm 0.06}$ from 24 to 150 R$_J$. The north-south thickness of the plasma sheet is usually well resolved at radial distances from 25 R$_J$ to 65 R$_J$ and is typically within the range 4 to 12 R$_J$. Beyond 65 R$_J$ the plasma sheet structure is no longer resolvable in the long-term, time-averaged data. Analysis of the local time dependence of the electron density yields no dusk to dawn asymmetry and no obvious local time dependence. However, the local time study is limited by relatively sparse data coverage, particularly in the 0400 to 0600 and 1800 to 2000 local times ranges.

TABLE OF CONTENTS

LIST OF FIGURES

CHAPTER I

INTRODUCTION

1.1. Statement of Intent

The goal of this study was to analyze the plasma wave data from the Galileo spacecraft to obtain a description of the average electron density in the night side magnetosphere of Jupiter. To obtain this goal, three methods were employed. The first analyzed the current sheet electron density dependence on radial distance from Jupiter. The second analyzed the magnetic dipole cross section of the plasma sheet. The last analyzed the local time dependence of the current sheet electron density searching, specifically, for asymmetry between the dawn and dusk regions. These methods developed a three dimensional picture of the electron density averaged over long time intervals.

1.2. A Brief History of the Galileo Mission

The Galileo spacecraft was conceived following the success of the 1979 Voyager flybys of Jupiter. Launched from the space shuttle, Atlantis, on October 18, 1989, Galileo flew by Earth, Venus, and two asteroids before arriving at Jupiter on December 7, 1995. The prime mission, lasting from March 23, 1996 through November 9, 1997, included all orbits from local morning to local midnight. However, data collection continued in an extended mission until September 16, 2003 when the spacecraft was purposely crashed into Jupiter to prevent accidental contamination of the Galilean satellites, especially Europa. The electron density data set obtained from these measurements extended from May 23, 1996 to November 4, 2002.

Included onboard Galileo was a plasma wave instrument designed and constructed at the University of Iowa. The instrument consisted of an electric dipole antenna, a search coil magnetic sensor, a swept frequency receiver, and a wideband

receiver. The frequency response of the electric dipole system was from 5.62 Hz to 5.65 MHz. The search coil magnetometer had a frequency response from 5.62 Hz to160 kHz. The swept frequency receiver generated a power spectrum every 37.33 seconds. The data in each time period was represented as an intensity versus frequency spectrum. Electron plasma densities were calculated from a cutoff at the electron plasma frequency, and from an emission line at the upper hybrid resonance frequency.

1.3. Work Done in the Prime Mission

During the prime mission electron plasma density determinations were performed by a former graduate student, Dr. Jay Ansher, under the direction of Professor Donald Gurnett. It was found that the mean electron density varied with radial distance from Jupiter as $(1/r)^{2.14\pm0.01}$ from 20 to 150 R_J and as $(1/r)^{6.55\pm0.05}$ from 6 to 20 R_J. The prime mission covered orbits from local morning to midnight. The prime mission work formed the basis of Ansher's study, and, as a result, most of the analysis programming and data archiving had been completed.

The work accomplished as part of this thesis consisted of processing the data from the extended missions and correcting various errors present in the data set from the prime mission. Fortunately, funding was provided through the NASA Jet Propulsion Laboratory to continue the study through the summer of 2004. To this end, the entire night side data set was processed and analyzed.

1.4. Jovian Magnetosphere Theory

The Jovian magnetosphere has three characteristics that distinguish it from Earth. One is Jupiter's larger magnetic moment, 1.6×10^{11} T·km^3 versus 8.0×10^6 T·km^3 for Earth, a difference of more than four orders of magnitude. As a result, the Jovian magnetosphere is much larger than that of Earth. Second, Jupiter's equatorial radius is 11 times greater than that of Earth, 71,492 versus 6,378 km for Earth. The larger radius combined with Jupiter's shorter rotation period, 9.925 hours, less than half that of Earth,

produces much larger centrifugal forces on the magnetospheric plasma. For this reason, Jupiter's rotation is the principal source of energy for the magnetospheric plasma whereas the solar wind is the principal energy source for plasma in the Earth's magnetosphere. Third, the Jovian magnetosphere has a strong internal plasma source. At Earth, the solar wind and the Earth's ionosphere are the primary sources of plasma. The primary plasma source in the Jovian magnetosphere is the Galilean moon, Io. Io orbits deep within the magnetosphere at roughly six Jovian radii, R_J. In addition, its orbit is constantly perturbed by the other Galilean satellites, particularly Ganymede. These perturbations lead to tidal stresses on Io which stress and heat its mantle. This heating causes volcanic activity that varies over time but results in a mean mass ejection of about one ton per second into the Jovian magnetosphere. This ejected gas is then ionized by electron collisions or photoionization, creating a torus of plasma around Jupiter known as the Io plasma torus. This torus is shown with respect to the larger magnetospheric structures in Figure A.1. Near Jupiter the plasma rotates near synchronously with the planet. This rapid rotation generates a centrifugal force on the plasma that drives it radially outward via interchange motions which disperse the plasmas throughout the magnetosphere. These interchange motions may be conceptualized as the interchange of flux tubes from the inner regions of the magnetosphere to the outer regions.

Electromagnetic waves are generated from a number of sources within the Jovian magnetosphere. For this study the principal interest has not been the source of such radiation, but rather the information such waves provides about the electron density. To achieve this end, the most useful form of radiation is trapped continuum radiation. Trapped continuum radiation ranges in frequency from less than 10^3 Hz to about 10^4 Hz, and typically has a sharp, low frequency cutoff in the neighborhood of 10^3 Hz. The radiation is trapped by the sharp density increase that occurs at the Jovian magnetopause. This density increase leads to a sharp increase in the plasma frequency which prevents the escape of the continuum radiation from the low density region of the Jovian

magnetosphere. Since the radiation cannot propagate through this barrier, it is reflected and remains trapped in the magnetospheric cavity until it is either absorbed or escapes via energy gain or some other mechanism. This trapping process is illustrated in Figures A.2 and A.3. Figure A.2 illustrates how the radiation is trapped in the magnetosphere. Figure A.3 shows the expected frequency range of trapped continuum radiation. This illustration also shows the magnetopause cutoff with a 10^4 Hz plateau corresponding to the magnetopause plasma frequency. The right hand boundary of the trapped continuum radiation is caused by the plasma frequency increase at the Io plasma torus, which prevents the continuum radiation from penetrating the region inside approximately $20R_J$.

In the Jovian magnetosphere, cold plasma wave theory works very well for describing trapped continuum radiation since thermal effects are minimal and may be ignored. Electrons with their low mass are the primary species affecting the propagation of continuum radiation, as ions, being much heavier, are nearly stationary at these frequencies. Therefore, the properties of these waves are controlled almost exclusively by the electrons. Continuum radiation consists of left-hand ordinary (L-O) and right-hand extraordinary (R-X) free space modes of propagation. These two modes have the following cutoff frequencies:

$$\text{Right-hand (R-X) mode: } \omega_{R=0} = \frac{|\omega_{ce}|}{2} + \sqrt{\left(\frac{\omega_{ce}}{2}\right)^2 + \omega_{pe}^2} \qquad (1.4.1)$$

$$\text{Left-hand (L-O) mode: } \omega_{L=0} = -\frac{|\omega_{ce}|}{2} + \sqrt{\left(\frac{\omega_{ce}}{2}\right)^2 + \omega_{pe}^2} \qquad (1.4.2)$$

where $\omega_{R=0}$ and $\omega_{L=0}$ signify the right and left hand mode cutoff frequencies respectively, ω_{ce} is the electron cyclotron frequency, and ω_{pe} is the plasma frequency.

Throughout most of the Jovian magnetotail, the plasma frequency is always greater than the cyclotron frequency by an order of magnitude or more, so the index of refraction equation can be approximated to first order by ignoring ω_{ce}. However, because of the cyclotron frequency is non-zero, the R-X mode cutoff is slightly higher than the electron plasma frequency and, thereby terminates before the L-O mode on a frequency spectrum. This cutoff relationship is illustrated in Figure A.4 by a plot of the index of refraction, n, versus frequency, ω. As shown the L-O mode terminates at the plasma frequency, ω_p, because at this point the index of refraction goes to zero. As the wave frequency, f, of the radiation approaches the plasma frequency, f_p, this cutoff occurs and is expressed by thé following, simplified index of refraction equation:

$$n^2 = 1 - \frac{f_p^{\,2}}{f^2} \Rightarrow n = \sqrt{1 - \frac{f_p^{\,2}}{f^2}} \qquad (1.4.3)$$

where n is, again, the index of refraction.

The propagation cutoff at f_p provides a clear feature in the spectrum at which to measure the plasma frequency, and, hence, determine the electron density. Since the plasma frequency, f_p, is directly related to the square root of the electron number density, n_e, a simple calculation yields the equation for the electron density:

$$f_p = \frac{1}{2\pi} \sqrt{\frac{n_o e^2}{\varepsilon_o m_e}} = 8980 \sqrt{n_e} \, Hz \qquad (1.4.4)$$

or

$$n_e = \left(\frac{f_p}{8980}\right)^2 cm^{-3} \qquad (1.4.5)$$

where n_e is the electron density in cm^{-3}, e is the electron charge, ε_o is the permittivity of free space and m_e is the electron mass.

Close to the planet the continuum radiation method of measuring the electron density fails because the rapid increase in the plasma frequency with decreasing radial distance prevents the radiation from propagating in the region of $r < 20$ R_J. This increase

is observed as one traces the plasma frequency line from left to right in Figure A.3. At radial distances less than approximately 20 R_J, the plasma frequency is beyond the upper frequency limit of the trapped continuum radiation. This upper frequency limit is controlled by both the magnetopause and solar wind plasma frequencies, above which the continuum radiation escapes from the magnetosphere (see Figure A.3). Fortunately, an emission line relating to the upper hybrid resonance frequency is usually identifiable from the electric field spectra in this inner region. By measuring the frequency of the upper hybrid emission line and with knowledge of the cyclotron frequency from the magnetometer data, the plasma frequency can be calculated using the following simple relationship:

$$f_{uh} = \sqrt{f_c^2 + f_p^2} \Rightarrow f_p = \sqrt{f_{uh}^2 - f_c^2} \qquad (1.4.6)$$

where f_{uh} is the upper hybrid frequency, f_c is the electron cyclotron frequency, and f_p is the plasma frequency.

To illustrate the low frequency cutoff of trapped continuum radiation, consider the intensity versus frequency spectrum shown in Figure A.5. Notice the sharp intensity drop-off at approximately 10^3 Hz which is marked by an arrow. The low frequency side of this characteristic intensity peak marks the low frequency cutoff of the trapped continuum radiation and, therefore, the plasma frequency. By examining Figure A.6, which shows a frequency versus time spectrogram of Galileo plasma wave data, one notices how this 10^3 Hz cutoff extends across an entire day. The low frequency portion of the trapped continuum radiation is the yellowish band fluctuating about 10^3 Hz. The low frequency cutoff is marked by the white line traced across the spectrogram. This cutoff should not be confused with the lower frequency white line marked f_{ce} which is the electron cyclotron frequency computed from the on-board magnetic field measurements.

To analyze spatial variations in the plasma frequency, a coordinate system must be employed to describe the spacecraft's location relative to the current sheet in the Jovian magnetotail. This coordinate system can either be based on the marked change in

the magnetic field polarity at the current sheet, or on a model that describes the mean location of the current sheet. In this investigation, both methods are used.

The current sheet is a current that flows in a narrow sheet across the magnetotail from dusk to dawn. Existing near the center of the plasma sheet, the current sheet is characterized by a reversal in the sunward (x) component of the magnetic field. This polarity switch in the sunward component of the magnetic field can be used to identify the center of the sheet. The center also corresponds to the densest portion of the plasma sheet, as the plasma pressure dominates the magnetic field pressure in this region. Correlating the plasma wave data with the current sheet is usually straightforward. The UCLA magnetometer data clearly shows the reversal of the field marking the center of the plasma sheet. Associating this time with the plasma wave measurement yields peak densities for the plasma sheet fulfilling one of the goals of this study.

The second method of identifying the current sheet was based on a model developed by Krishan Khurana of UCLA. This model provided a means to orient density measurements by mapping the current sheet's displacement from a reference plane using Jupiter-centered Solar Magnetic or JSM coordinates. This measure was necessary since the Jovian current sheet location changes with increasing distance downtail from the planet (see Figure A.7). Like Geocentric Solar Magnetospheric, GSM, coordinates used at Earth, JSM coordinates were defined as follows:

1. The origin was placed at Jupiter's center.

2. The x-axis was defined by the line between Jupiter and the Sun and was positive towards the Sun.

3. The z-axis was defined to be positive in the same direction as the northern magnetic pole.

4. The y-axis was defined to be perpendicular to the magnetic dipole cross section and positive opposite the direction of revolution about the Sun.

Using the JSM coordinate system Galileo's position is located relative to the magnetic field of the planet. Near the planet the current sheet aligns itself with the azimuthal plane of the magnetic field instead of the equatorial plane of planetary rotation. As distance increases the current sheet changes alignment to that parallel to the plane of planetary rotation which is defined as the xy-plane in JSM coordinates. This process of realignment is referred to as hinging. Figure A.7 illustrates this hinging effect with a sketch of the magnetotail's xz cross section. Note that the xy-plane is illustrated as lying below the magnetotail. As the planet rotates the downtail region of the current sheet oscillates above and below this xy-plane. The hinge between the near-Jovian and downtail regions occúrs in the region between 15 and 30 R_J. The downtail shift in plasma is not instantaneous, so a region exists where propagation delay is important.

Khurana's model accounts for these phenomenon via a parameter fit based on Pioneer 10, Voyagers 1 & 2, and early Galileo magnetometer data. The following equations predict the mean current sheet separation distance, z_{cs}, from the JSM xy-plane:

$$z_{cs} = \rho \tan\left(\theta_{cs}\right)\left[\frac{x_o}{x}\tanh\left(\frac{x}{x_o}\right)\cos\left(\phi-\delta\right)-\cos\left(\phi-\pi\right)\right] \tag{1.4.7}$$

$$\theta_{cs} = 6.4^\circ + 3.2^\circ \tanh\left(\frac{\rho}{6}\right) \tag{1.4.8}$$

$$\delta = \pi - \frac{\Omega_J \rho_o}{v_o}\ln\left(\cosh\left(\frac{\rho}{\rho_o}\right)\right) \tag{1.4.9}$$

where the value θ_{cs}, the magnetic axis offset, is in degrees and is typically 9.6°; x is the position along the JSM x-axis; and ρ is Galileo's radial distance from Jupiter in the JSM xy-plane, $\rho = \sqrt{x_{JSM}^2 + y_{JSM}^2}$. The fitting parameters used are as follows: $x_o = -33.5\ R_J$ is the characteristic distance from Jupiter after which the current sheet is fully hinged; $\rho_o = 33.2\ R_J$ is the distance after which the propagation delay is significant; $v_o = R_J/h$ is the asymptotic value of the Alfvén velocity; and $\Omega_J = 0.63$ radians $(h)^{-1}$ is the angular rotation velocity of Jupiter; all in cylindrical coordinates. Subtracting the z_{cs} value from the z-

axis position of the spacecraft yields Galileo's distance from the plane of the current sheet, Δz

$$\Delta z = z - z_{cs} \qquad (1.4.10)$$

Now, with x, Δz, and the electron density calculated from the plasma frequency, a spatial description of the electron density for Jupiter's nightside magnetotail is obtained, fulfilling the second goal of this study.

The third goal of this study is to determine whether solar wind interactions affect the local time distribution of the electron plasma density. Influences from the solar wind are thought to change the plasma density by interacting with various currents present in the magnetosphere. These interactions lead to solar wind driven convection which is observed by the presence of field aligned currents (FAC's) in the magnetosphere. Furthermore, the presence of these currents indicates a strong interaction between the planetary system and the solar wind.

In 2001 Khurana published a study of Jovian magnetospheric currents using UCLA magnetometer data from Galileo. This study showed the presence of Region 1 and Region 2 field aligned currents. Region 1 currents ran from the north polar region to the south while Region 2 currents ran in the opposite direction. These FAC's do not extend beyond 30 R_J indicating that solar wind influences must penetrate deep into the Jovian magnetosphere. Moreover, analysis of azimuthal current measurements yielded an asymmetry in the divergence of such currents between the dusk and dawn regions. Specifically, the divergence was positive in the dusk region and negative in the dawn. This asymmetry was also present when analyzing the ratio of $\Delta B_\varphi / \rho B_\rho$ where B_φ is the azimuthal magnetic field and B_ρ is the radial field. This magnetospheric behavior prompted the third analysis of this study.

Analysis of the local time dependence of the electron density could not only support the magnetometer results but also complete the overall trend of electron density dependence. The main issue to address is the size of bins in radial distance and local time. Relatively sparse local time data coverage necessitates large, local time binning of data for good statistics. Furthermore, it is necessary to partition the radial bins by electron density behavior to prevent large variation from biasing the region. Despite this measure, electron density measurements still vary widely within radial bins. As a result, the data require a weighting function to further reduce biasing.

It became readily apparent that the easiest means of setting bin size and data weighting was to use the results from the previous analyses. Therefore, the hinge region demonstrated by the current sheet electron density trend was used to set the outer edge of the innermost bin. Also this density trend formed the basis of the data weighting model. Next, the end of plasma sheet structure seen in the spatial electron density analysis provided a reasonable breaking point between the middle and outermost bins. The ratio of the measured electron density to the weighting model was plotted for each bin such that the dusk to dawn density difference would be apparent by fractions greater or less than one.

CHAPTER II

DATA ANALYSIS PROCEDURES

2.1. Digitalization of Data

Before the electron density data can be analyzed, the low frequency cutoff of the trapped continuum radiation must be measured. On a frequency spectrum the cutoff is noted by a sharp drop in the intensity. The drop usually occurs between 100 and 1000 Hz. Each identified cutoff is assigned a quality index. These range from zero to three with zero being the most discernable. A quality index of zero indicates a sharply defined cutoff having a nearly vertical slope on the spectrum with little or no interference at either end of the transition. A quality index of one indicates a cutoff having a steep slope with some interference present at either or both ends. A quality index of two indicates a cutoff with a moderate slope and considerable interference which makes one or both ends difficult to identify. A quality index of three includes anything less distinguishable than index two. Cutoffs with quality indices of two or three are not used as their considerable uncertainty diminishes the credibility of the analysis.

Each spectrum provides a single measurement of the cutoff frequency. Each measurement is then combined with the quality index and ephemeris data for use in further analysis. The act of measuring the low frequency cutoff is done by a technician. Digitalization of each spectrum required approximately 30 seconds. As the instrument resolution is 37.33 seconds, the process of digitizing the information progresses in real time requiring hundreds of man-hours to complete the entire data set. The technician loads a group of spectra into an analysis program and proceeds one by one to mark the cutoff frequency using a mouse pointer on a computer screen. Each time interval now has a cutoff frequency value for use in density calculations and tracing the white line across composite frequency spectrograms like Figure A.6. As each group is completed, it

is transferred to a new network directory for verification. The process of verifying the data entails checking for the white line fit to the composite spectrogram's continuum radiation structure and confirming that the density values are consistent with the overall trend in the spectrogram.

Problems encountered with this process were mainly caused by human judgment. Each technician would use a slightly different process of determining the exact cutoff placement, which was expected as no two people think exactly alike. Such variations increased with the number of technicians working. Therefore, digitalization was limited to as few technicians as possible. Still, with multiple technicians involved, good communication between them maintained consistency throughout the data set. However, the data set was not without discrepancies. Solar wind data and processing errors not caught by verification became apparent after initial analysis and were resolved.

2.2. Current Sheet Electron Density Determination

As Jupiter rotates its magnetosphere oscillates every 9.925 hours causing the plasma sheet to sweep across the spacecraft twice per Jovian rotation. The greater of the calculated electron density values at the two current sheet crossings is used to determine the electron plasma density at the current sheet during that period. The reason both values are not used is theoretical as well as procedural. Theoretically, the greater value should be nearer to the exact center of the sheet. Procedurally, as the spacecraft's distance from the JSM xy-plane increases, the time interval between current sheet crossings decreases until the two crossings are indistinguishable. Due to the tilt of Jupiter's rotation axis relative to the ecliptic plane, such occurrences are relatively frequent in the data set. To use both crossings and, thereby, increase the number of points in the data set would have required significant time and resources to identify both points and make the distinction between them.

Inside 20 RJ, however, all data points are used as the significantly reduced number of data points in this region requires the use of all available data to obtain useful results. The number of useful upper hybrid cutoffs is rather low. The program "edanalysis" generates a log/log plot of the electron density versus radial distance using data from user selected sets. From this file's output, a best fit power law describing the average electron density within a given, radial distance range is calculated using a linear least squares fitting program.

2.3. Spatial Electron Density Determination

To determine spatial variation of the electron density in the magnetosphere the Khurana magnetosphere model is utilized. Using the UCLA magnetometer data, the azimuthal angle, δ, is calculated, and with this angle the Khurana model embedded in the "densityplot" program can predict the shift of the current sheet in the z_{cs} direction. Then by comparing the position of the satellite to this distance, a Δz value is calculated from equation 1.4.10, giving the satellite's location relative to the current sheet. Galileo's x and y coordinates were then used to compute a projected radial distance, $\rho = \sqrt{x_{JSM}^2 + y_{JSM}^2}$, with which to categorize the density measurement. Ten minute means for electron density are then calculated and the largest of these per Jovian rotation is used. This time period is used because it balanced processing time versus data volume. The selected value is then binned by radial distance and Δz value, and the binned values averaged. These bins are subsequently expressed as a color coded plot with the color spectrum indicating the electron plasma density.

2.4. Local Time Dependence Determination

To develop a description of the local time dependence parameters for weighting and binning the data were necessary. Results from the other analyses were used to establish these parameters. First, the current sheet progressions, established from the linear least squares fits, provided a model against which the data could be weighed.

$$n_m = 60 \times 10^9 \left(\frac{1}{r}\right)^{7.5 \pm 0.4} + 17 \times 10^2 \left(\frac{1}{r}\right)^{2.08 \pm 0.06} \tag{2.4.1}$$

The variable, n_m, was the model electron density, and r was the radial distance from Jupiter. Second, the spatial electron density results offered a means to divide the data into useful bins. The end of the hinge region bounded the inner bin. While the disappearance of plasma sheet structure could have been used to mark the end of the mid-range bin, this bin extended 5 R_J further to 70 R_J to enhance bin population. The last bin, including data located further downtail than $70R_J$, represented the deep tail. Four local time bins covered the night side of the planet. The focus of this analysis was the density difference between the dusk and dawn regions. The two intermediate bins served to establish a trend, if one existed, between the dusk and dawn regions. The final analysis was expressed as a polar intensity plot with the color spectrum illustrating the mean ratio of measured electron number density to the model electron number density,

$$Color \propto \left\langle \frac{n_e}{n_m} \right\rangle \tag{2.4.2}$$

where n_e is the measured electron number density and n_m is the model electron number density.

CHAPTER III

RESULTS

Total coverage in the final data set spans a time period of six and a half years and covers radial distances from 6 R_J to 150 R_J and local times from 2000 hours in the local evening through 0400 hours in the local morning. Figure A.8 illustrates the orbital path of Galileo for the entire mission. Green trajectories signify time periods where data exist. Again, for regions greater than approximately 20 R_J, not all data are used because good data density required elimination of measurements with poor quality indexes.

Consider first the current sheet density plots shown in Figures A.9 and A.10. Notice the two separate regions. One can discern the Io torus at 6 R_J in Figure A.9, indicating the density around the before mentioned source. The density profile through the inner region is not uniformly continuous because of the limited number of data points. Now consider Figure A.10. As radial distance increases one notices a distinct break in the electron density profile around 24 R_J. This break apparently corresponds to the hinge in the Khurana current sheet model. Further downtail of this region, the spread in density values broadens as radial distance increases. Applying a linear least squares fitting routine to the data on each side of the hinge region individually shows that the electron density varies as $(1/r)^{7.5\pm0.4}$ for radial distances from 6 to 24 R_J and as $(1/r)^{2.08\pm0.06}$ from 24 to 150 R_J (see Figure A.10). These values are similar to the prime mission results, $(1/r)^{6.55\pm0.05}$ and $(1/r)^{2.14\pm0.01}$, respectively. Note that the uncertainties in the power laws are for the line fit and are not representative of the scatter in the data. Uncertainties introduced by the digitalization process change slightly with the person processing the data as well as with the data quality. Actual uncertainties in the electron density measurements are estimated to be approximately 16%, though the actual number will vary somewhat depending on the mix of data quality indices. Overall, the electron

density was greatest in the Io torus, 4×10^3 cm^{-3}, and least in the distant magnetotail, 10^{-2} cm^{-3}.

Next, consider the spatial density plots, Figures A.11, A.12, and A.13. The plasma sheet structure is well defined to a distance of 40 R$_J$ as seen in Figure A.11. Figure A.12 shows that the plasma sheet structure diminishes after 45 R$_J$ and disappears completely by 65 R$_J$. The lack of downtail structure is illustrated in Figure A.13. The characteristic taper of the sheet moving away from the planet forms the predicted, distinctive boundary between the plasma sheet and the high latitude magnetotail. The plasma sheet varies in thickness from 4 to 12 R$_J$. Further than 65 R$_J$ downtail, the plasma sheet has no discernible structure and little electron density variation, less than an order of magnitude. This lack of structure seems due to an absence of spatial structure in the distant magnetotail.

Unlike the spatial density plot, the local time dependence plot, shown in Figure A.14, has no discernable structure or trend. While dusk to dawn density differences do exist between radially similar bins, this difference is half an order of magnitude or less and ratios in both regions are less than one. Moreover, the intermediate bins show no trend consistent with the dusk to dawn density difference. When comparing the intermediate bin density variations between the mid-range and downtail radial groups, such variations are opposite one another. This lack of consistency leads to the conclusion that either no dusk to dawn variation exists or this method is insufficient to resolve such information. The latter is strongly suspected due to the relatively sparse data coverage, specifically, the inadequate coverage from 1800 to 2000 and 0400 to 0600 hours local time.

All plots incorporate long time averages somewhere in their analysis. For the current sheet densities, the time averaging occurs in the linear least squares fitting of the data. For the spatial density and local time dependence plots the time averaging occurs when the individual bins are compiled. These time averages act to eliminate short time

scale variations and structures present in the data. Modification of present methods and greater spatial data density would be necessary to study short time scale variations.

CHAPTER IV

CONCLUSIONS

Two distinct regions of the Jovian plasma sheet can be identified in the electron density data, one less than 24 R_J and another greater than 24 R_J The transition point at 24 R_J is not precise because of the dynamic nature of the magnetosphere and varies as much as ±5 R_J. However, comparisons with the Khurana's magnetic field model show that 24 R_J marks the approximate center of the plasma sheet hinge region. The hinge center signifies a distinct change in the system's behavior. Near the planet a combination of the upper hybrid frequency, f_{uh}, and plasma frequency, f_p, measurements are used to determine the electron density. Downtail of the hinge region electron density calculations solely use plasma frequency measurements. The resultant radial density profile varied as $(1/r)^{7.5\pm0.4}$ from 6 to 24 R_J. Beyond 24 R_J the radial electron density profile varied as $(1/r)^{2.08\pm0.06}$. Near Jupiter the plasma associated with the Io torus is observed through the upper hybrid frequency calculations. Overall, electron densities varied from approximately 4×10^3 cm^{-3} in the densest region of the Io torus to 10^{-2} cm^{-3} in the distant magnetotail. The radial distances covered ranged from approximately 6 R_J, near the inner edge of the Io torus, to 150 R_J. The local times surveyed extended from about 2000 hours local evening, through local midnight, to about 0400 hours local morning.

The spatial dependence of the electron density exhibits a well defined structure characteristic of the plasma sheet from 18 R_J to 45 R_J. The north-south thickness of the plasma sheet is typically in the range 4 to 12 R_J. Downtail of 45 R_J, plasma sheet structure disappears completely beyond approximately 65 R_J. This lack of downtail structure in the plot is attributed to a lack of structure in the distant tail.

Local time dependence is not demonstrated by the analysis. However, some inconclusiveness remains from the local time analysis as the sparse data coverage in

some local time ranges could diminish the accuracy of the results. Specifically, the data set only extends from 2000 to 0400 hours via local midnight which effectively halves the dusk and dawn bins.

Long time scale averaging removes short term variations thus making the spatial variations smaller than actual. However, the overall large scale variations are believed to be accurate. Data consistency between the prime mission period and the extended mission period was reasonable within margins of uncertainty. While the linear fit uncertainties between the two studies do not overlap, the approximately 16% uncertainty in the plasma frequency measurements bring these results into agreement.

APPENDIX

Figure A.1.   This sketch illustrates the magnetosphere of Jupiter and shows the relative

locations of the magnetopause, planetary magnetic field, plasma sheet, and

Io torus.

JUPITER

BOW SHOCK

MAGNETOSHEATH

MAGNETOPAUSE

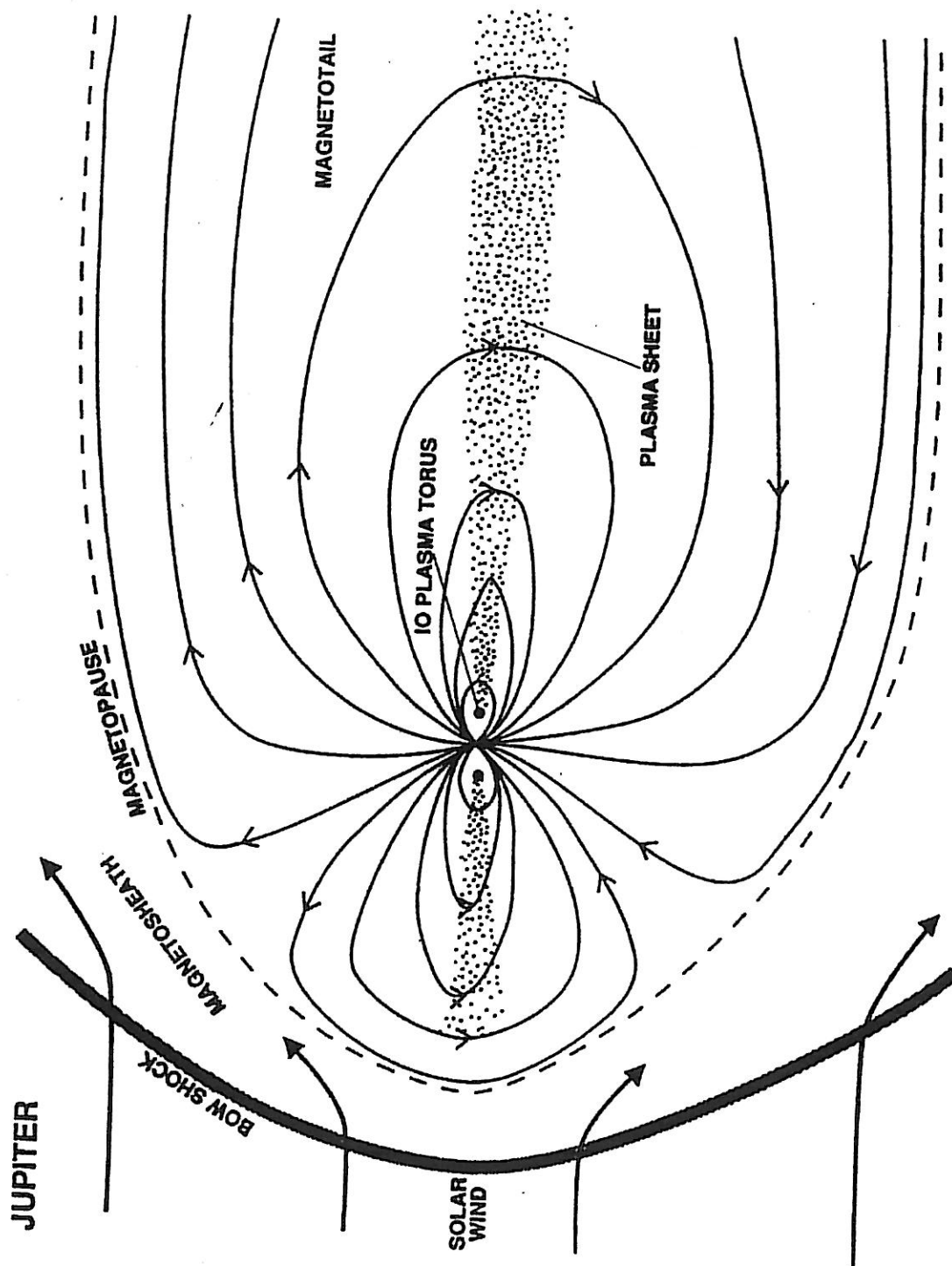SOLAR WIND

MAGNETOTAIL

IO PLASMA TORUS

PLASMA SHEET

Figure A.2. This sketch illustrates the reflection of radio waves at the magnetopause and the resulting trapping of continuum radiation. The radiation is trapped in regions where the local electron plasma frequency is below the magnetopause plasma frequency.

A-G97-237

MAGNETOPAUSE

LOBE

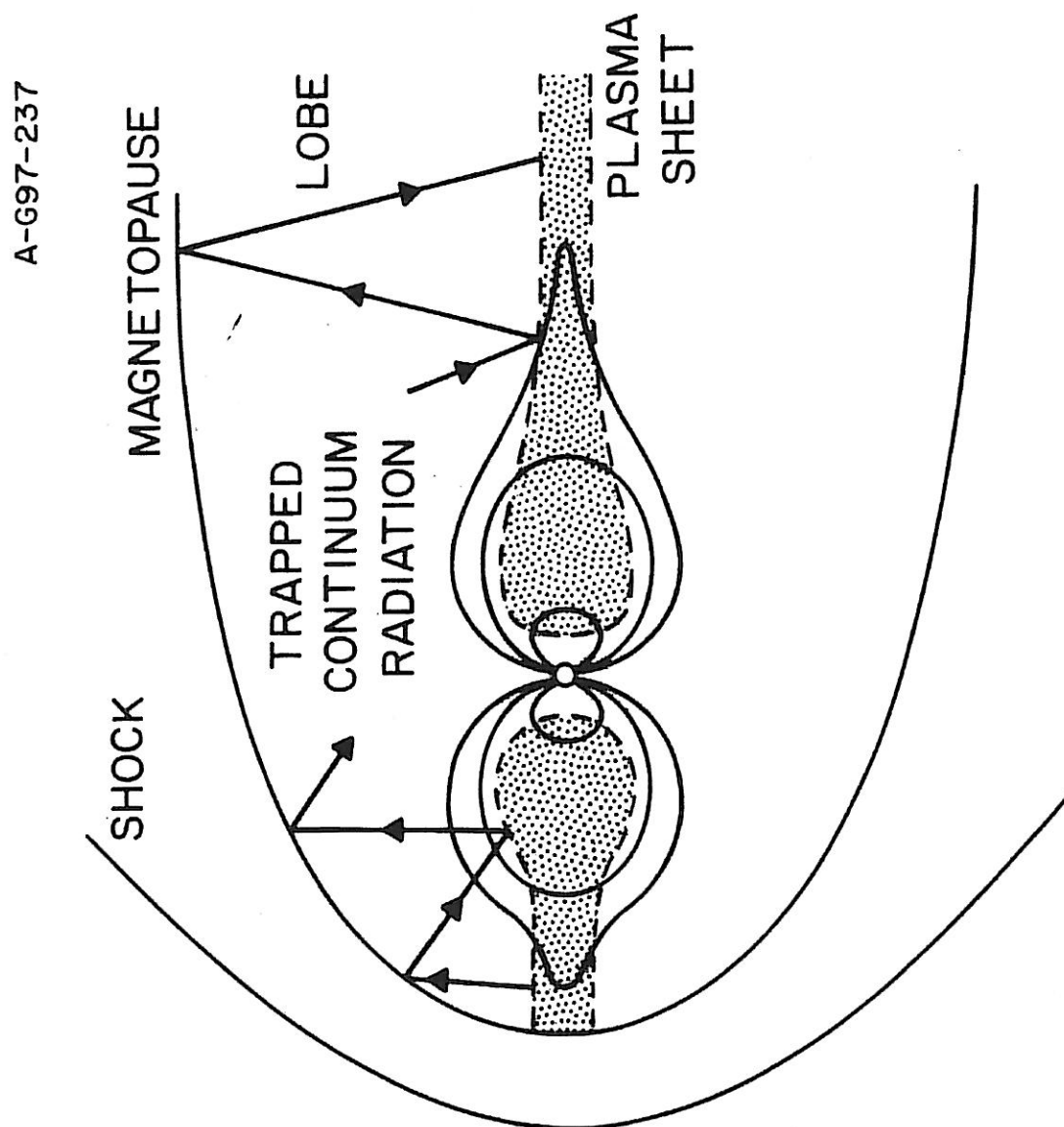PLASMA SHEET

SHOCK

TRAPPED CONTINUUM RADIATION

Figure A.3.   This plot of the plasma frequency versus radial distance from Jupiter

illustrates the principle involved in the use of trapped continuum radiation

to determine the electron plasma frequency. Also shown are the plasma

frequencies characteristic to the boundaries of the trapped continuum

radiation.

A-D79-358-1
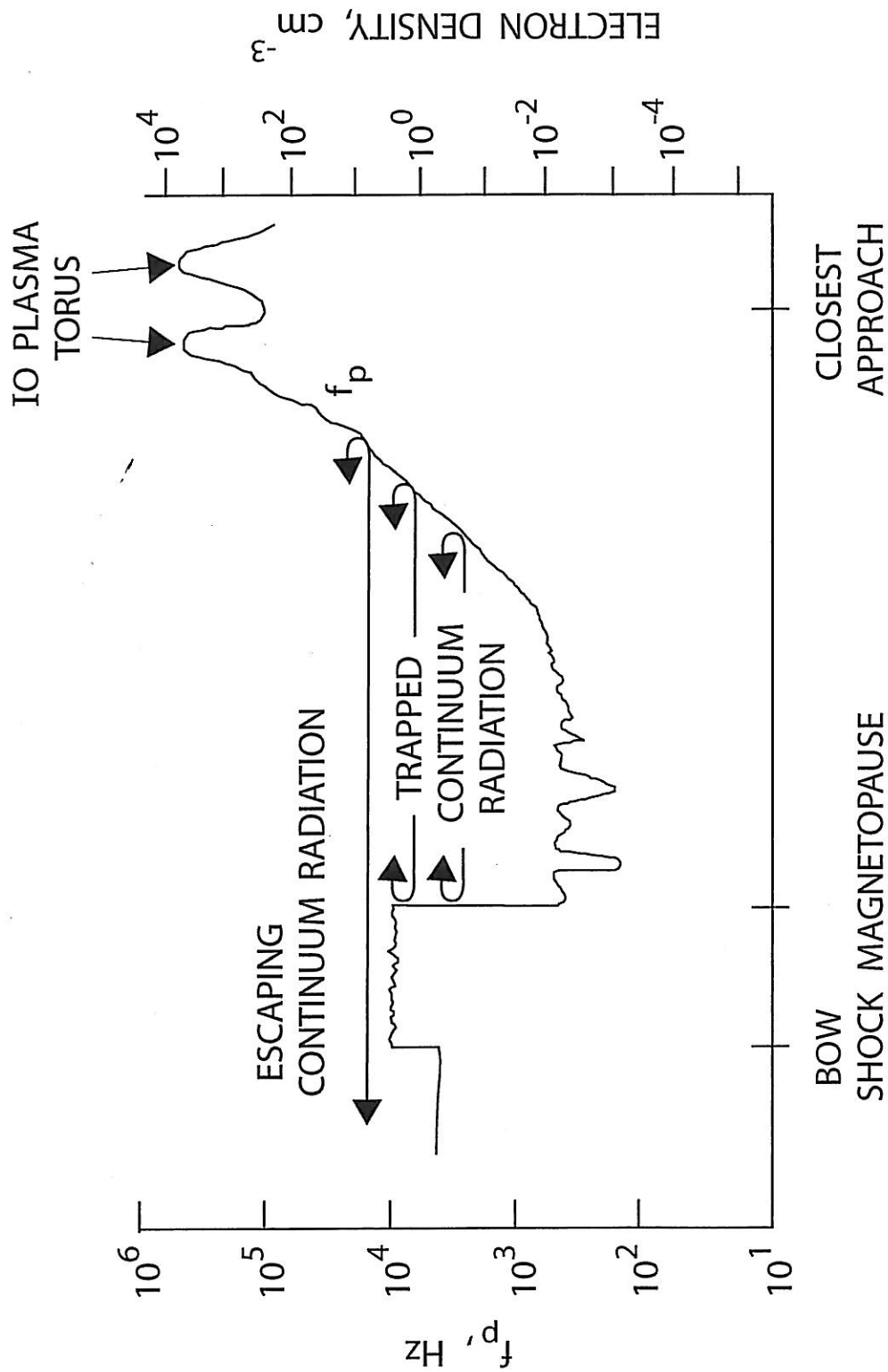
Figure A.4.   This illustration shows the index of refraction as a function of frequency

for the L-O and R-X modes of propagation. Notice the location of the

electron cyclotron frequency, ω_c, in relation to the two modes of

propagation. Also notice that the L-O mode cuts off at the plasma
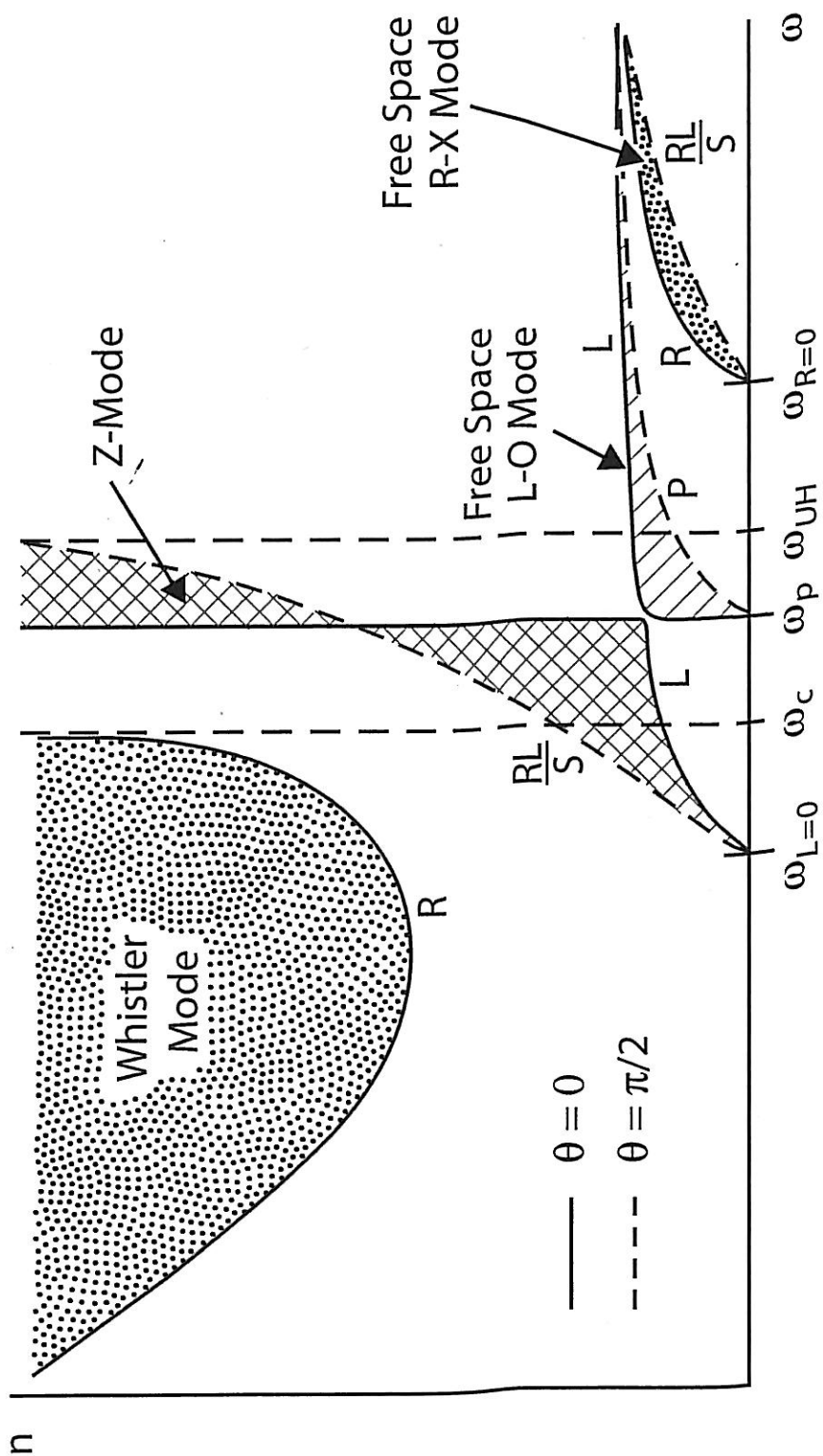
frequency ω_p.

Figure A.5.   This plot shows the electric field spectral density as a function of
frequency for a specific time, 00:18:09.529, June 1, 1997. Notice the
sharp drop at approximately 10^3 Hz which is marked by the arrow. This
change marks the plasma frequency.

1997 152 (June 1) 00:18:09.529
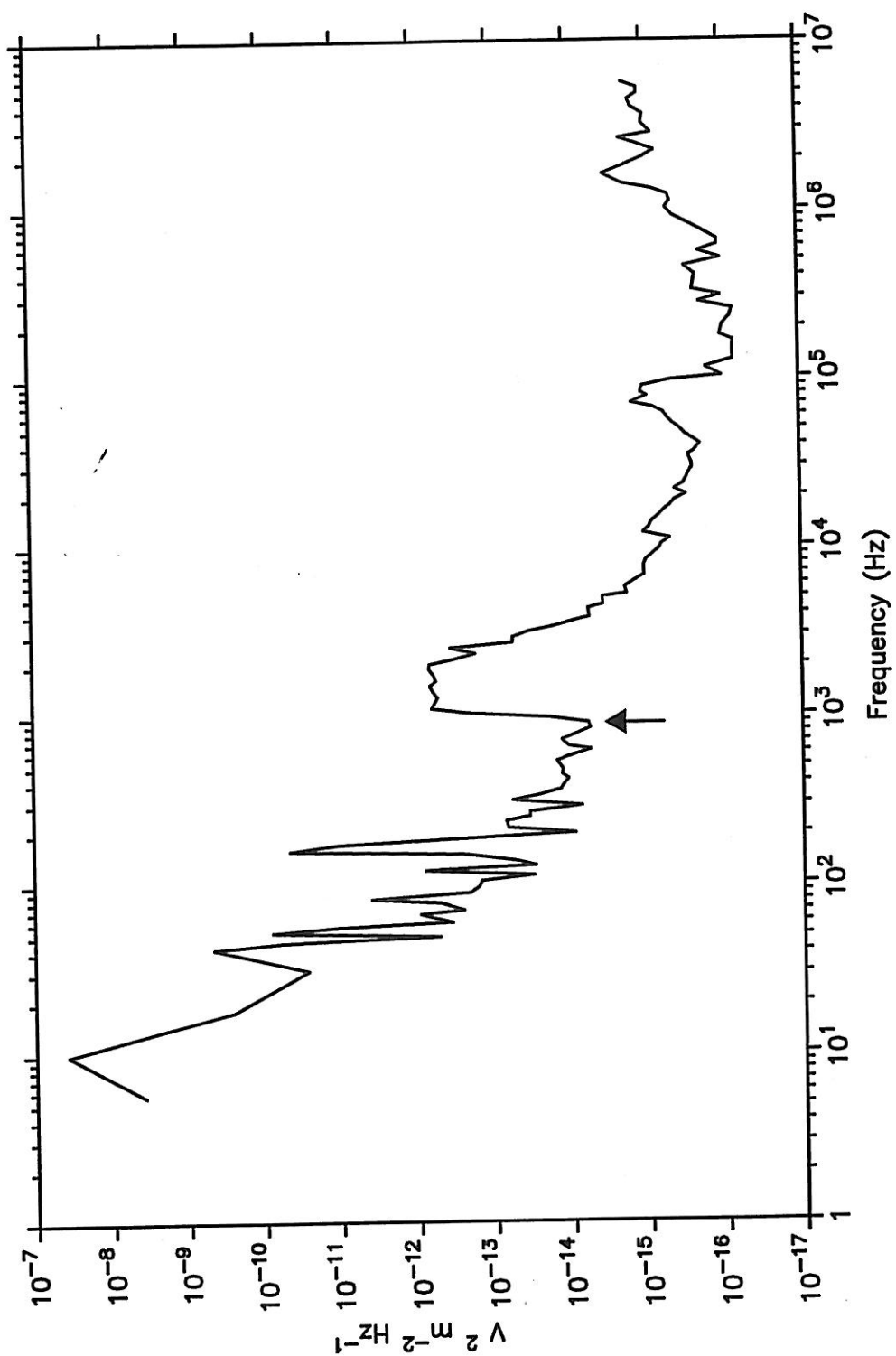Galileo PWS – Electric

Figure A.6.   This frequency-time spectrogram shows a one day sampling of the data

set. As the time resolution of the spacecraft is 37.33 seconds, this

composite represents about 2300 spectrum measurements. The white line

centered near 10^3 Hz is the electron plasma frequency. The other white

line is the electron cyclotron frequency, which is determined from the on-

board magnetic field measurements. The yellow band is the lower band of

the continuum radiation.
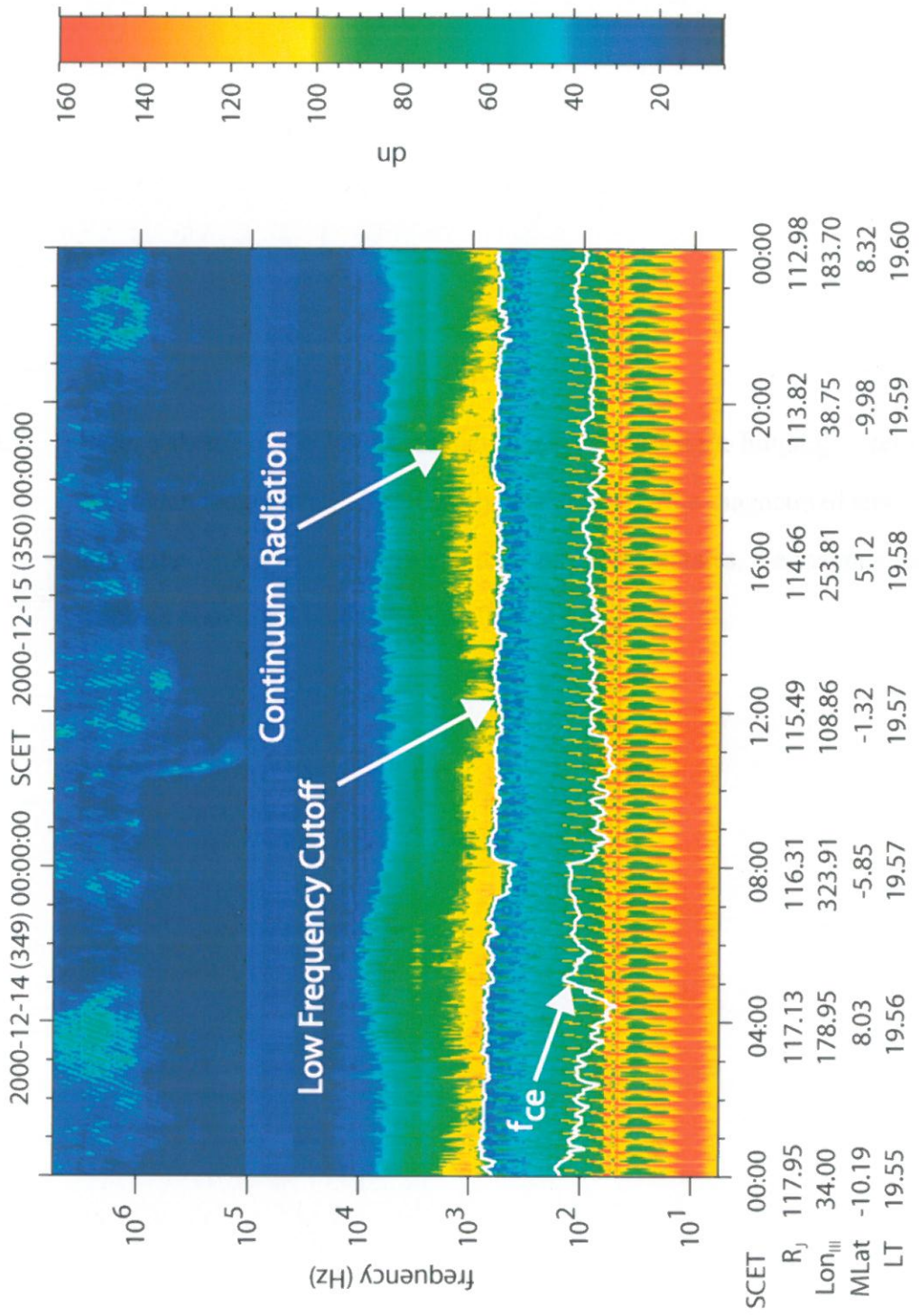
Galileo PWS Jupiter Impact

A-D05-003-2

Figure A.7.   Here, a sketch of the Jovian magnetic field illustrates the hinging effect of

the Jovian magnetotail. Specifically, it shows that the magnetotail sits

above the JSM xy-plane shown in red. As Jupiter rotates, the magnetotail

wobbles above and below the xy-plane.

A-D05-095-2

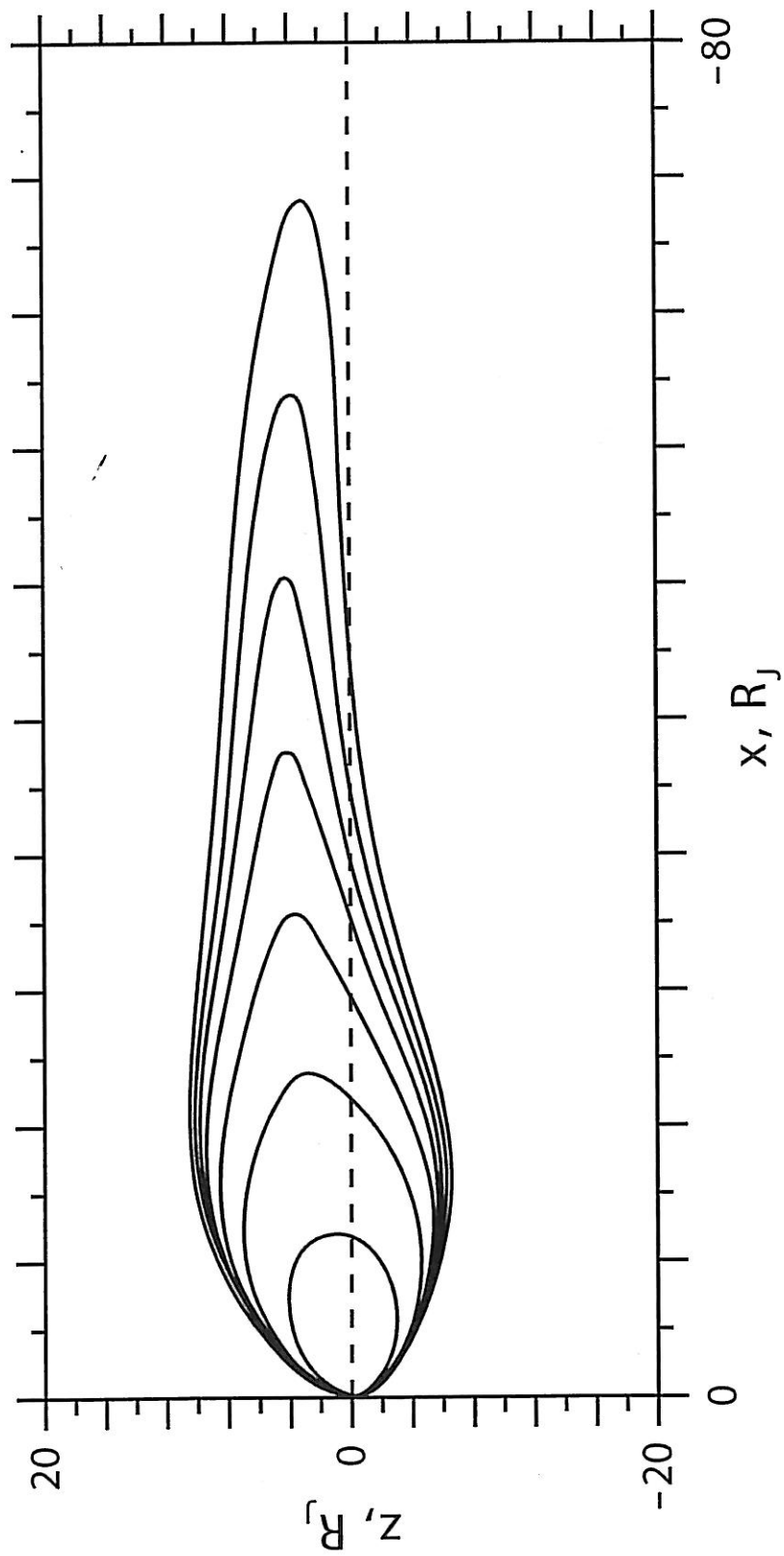Khurana's Jovian Magnetic Field Model

Figure A.8.   The Galileo data coverage for the entire mission is illustrated in this trajectory plot. The Voyager 2 model for the magnetopause is drawn in black. Processed data are shown in green. For this investigation only data with x values less than zero have been analyzed.
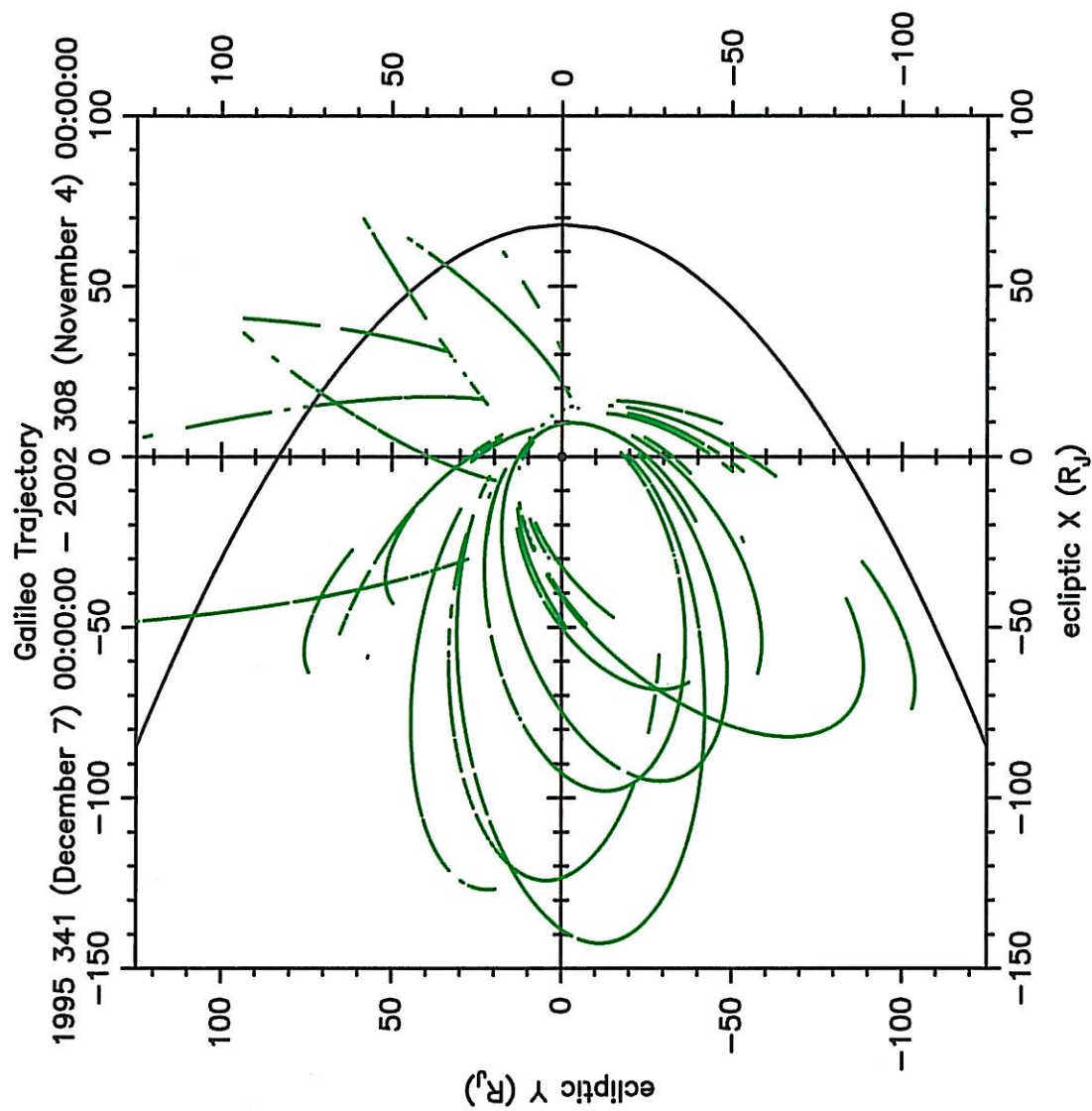
Tick marks every 10.0 days

Galileo Trajectory

1995 341 (December 7) 00:00:00 – 2002 308 (November 4) 00:00:00

ecliptic X (R_J)

ecliptic Y (R_J)

Figure A.9.   This log/log diagram illustrates the electron density values for the near
Jovian region. Notice the peak at approximately 6 R_J. The peak signifies
the highest density region of the Io plasma torus.

1995 001 (January 1) 00:00:00 – 1998 001 (January 1) 00:00:00

Radial distance (R_J)
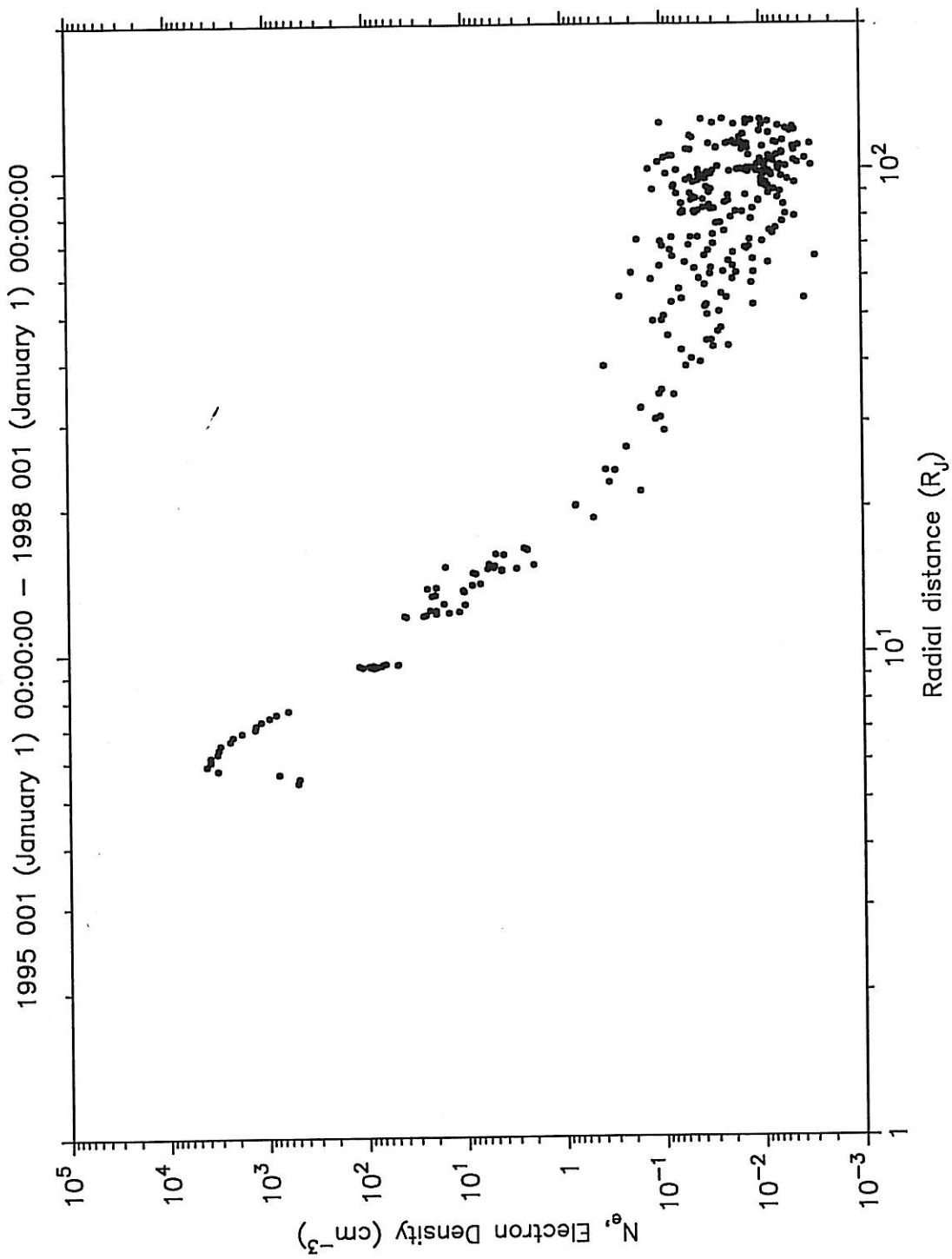
N_e, Electron Density (cm^{-3})

Figure A.10.   This log/log plot of the electron density versus radial distance illustrates

the data coverage as well as the change in data behavior at approximately

24 R_J. The near Jovian group has fewer points because of limited

availability of upper hybrid data. The electron density in this region, 6 to

24 R_J, varies as $(1/r)^{7.5\pm0.4}$. The data in the magnetotail, beyond 24 R_J, are

generated from the greater of two averaged values obtained at the two

current sheet crossings that occur during each Jovian rotation. The

electron density in this region varies as $(1/r)^{2.08\pm0.06}$.

Galileo Plasma Wave Data Current Sheet Densities

1996 175 (June 23) 16:15:00 – 2002 307 (November 3) 20:15:00

$\left(\frac{1}{r}\right)^{7.5\pm0.4}$

$\left(\frac{1}{r}\right)^{2.08\pm0.06}$

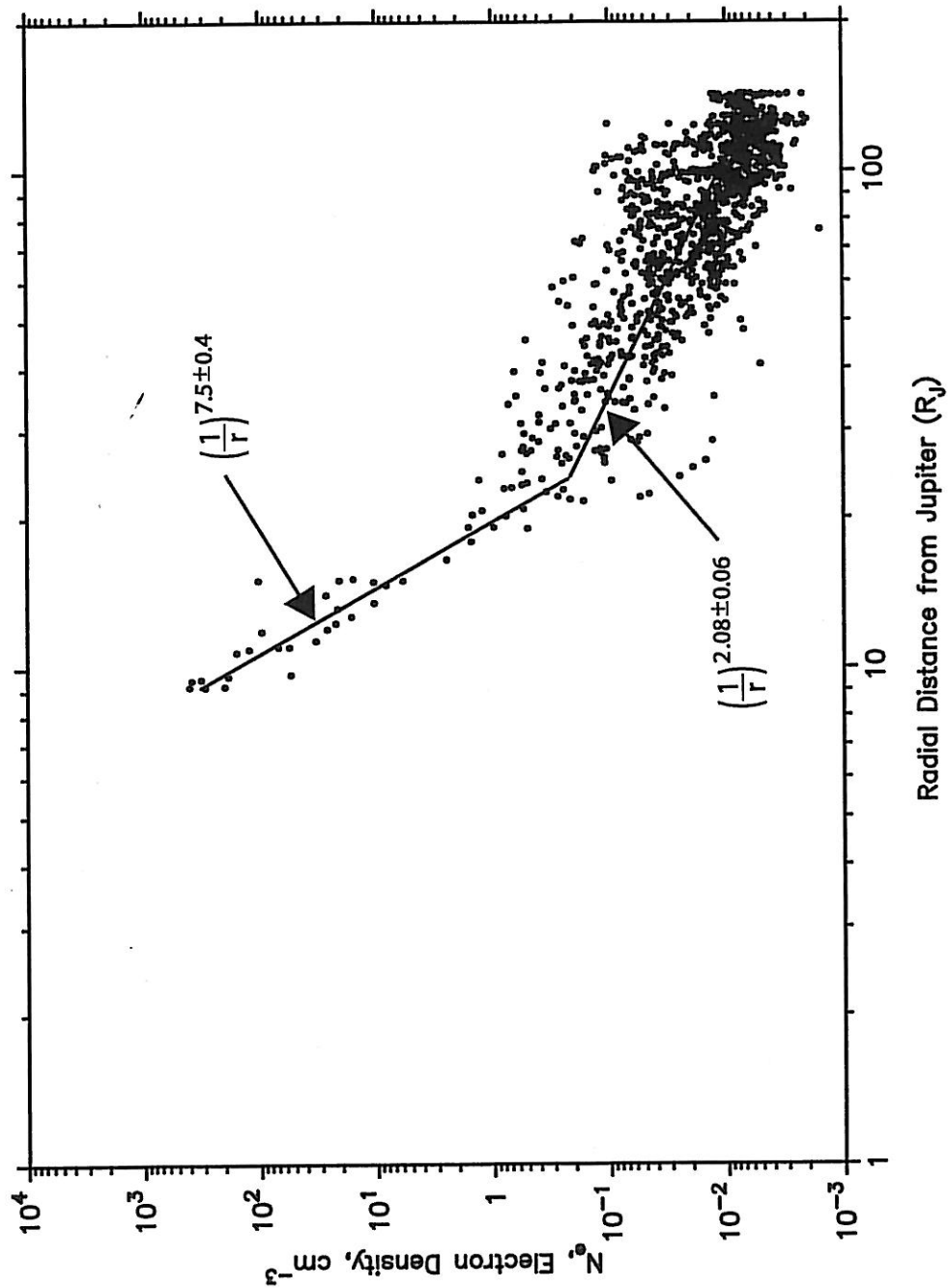Radial Distance from Jupiter (R_J)

N_e, Electron Density, cm^{-3}

Figure A.11. The spatial dependence of electron plasma density is illustrated in this
intensity plot. The relative z-axis position, Δz, and the radial distance
along the JSM x-axis define the spatial bins. Color indicates the electron
density. Notice the well defined structure of the plasma sheet between
approximately 18 and 40 R_J.

1996 144 (May 23) 00:00:00 – 2002 308 (November 4) 00:00:00

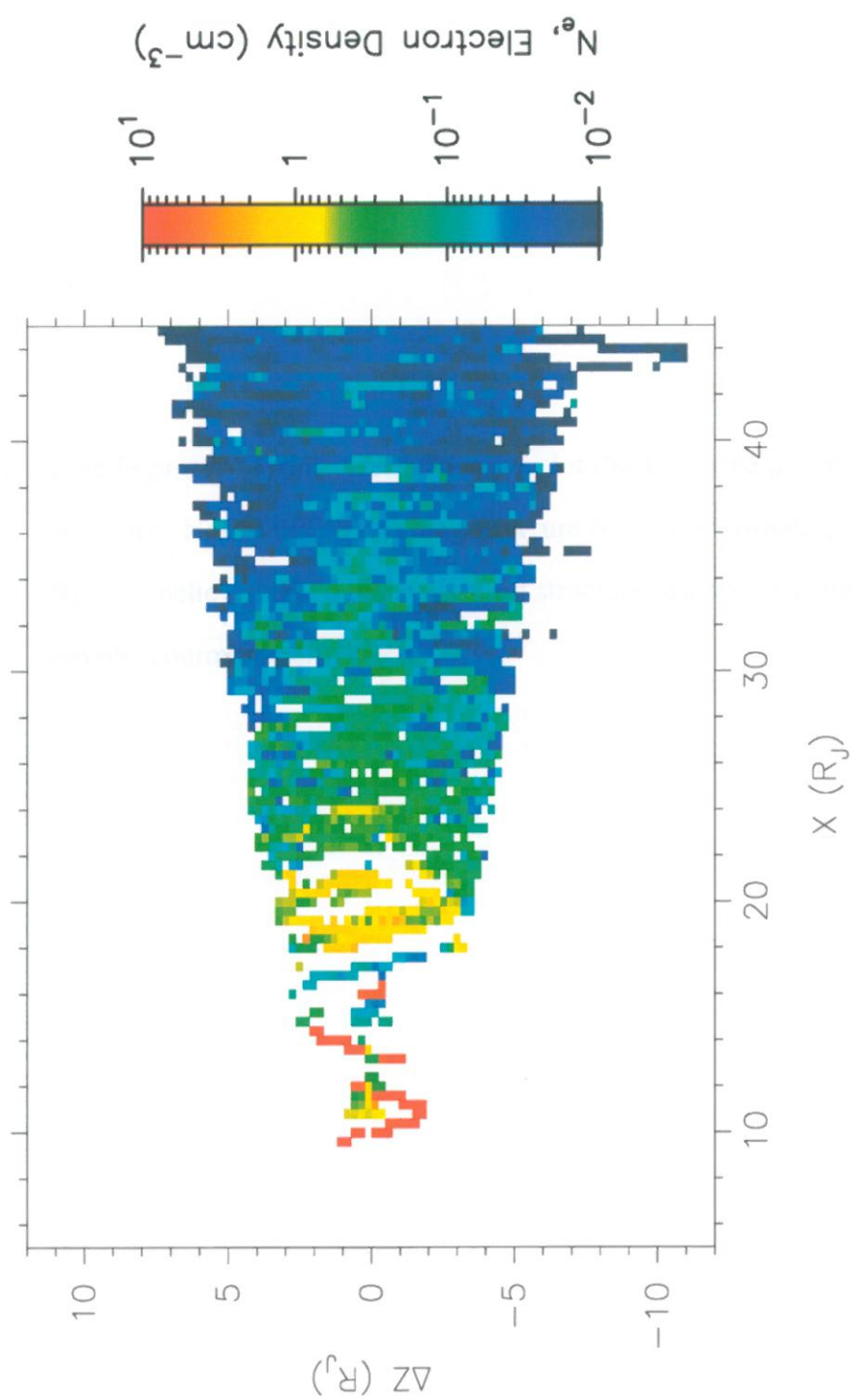N_e, Electron Density (cm^{-3})

Figure A.12   Like Figure A.11, this electron density plot illustrates the plasma sheet

structure. Notice the diminishing structure from approximately 45 to 65

R_J. It is believed that the plasma sheet structure disappears completely

beyond approximately 65 R_J.

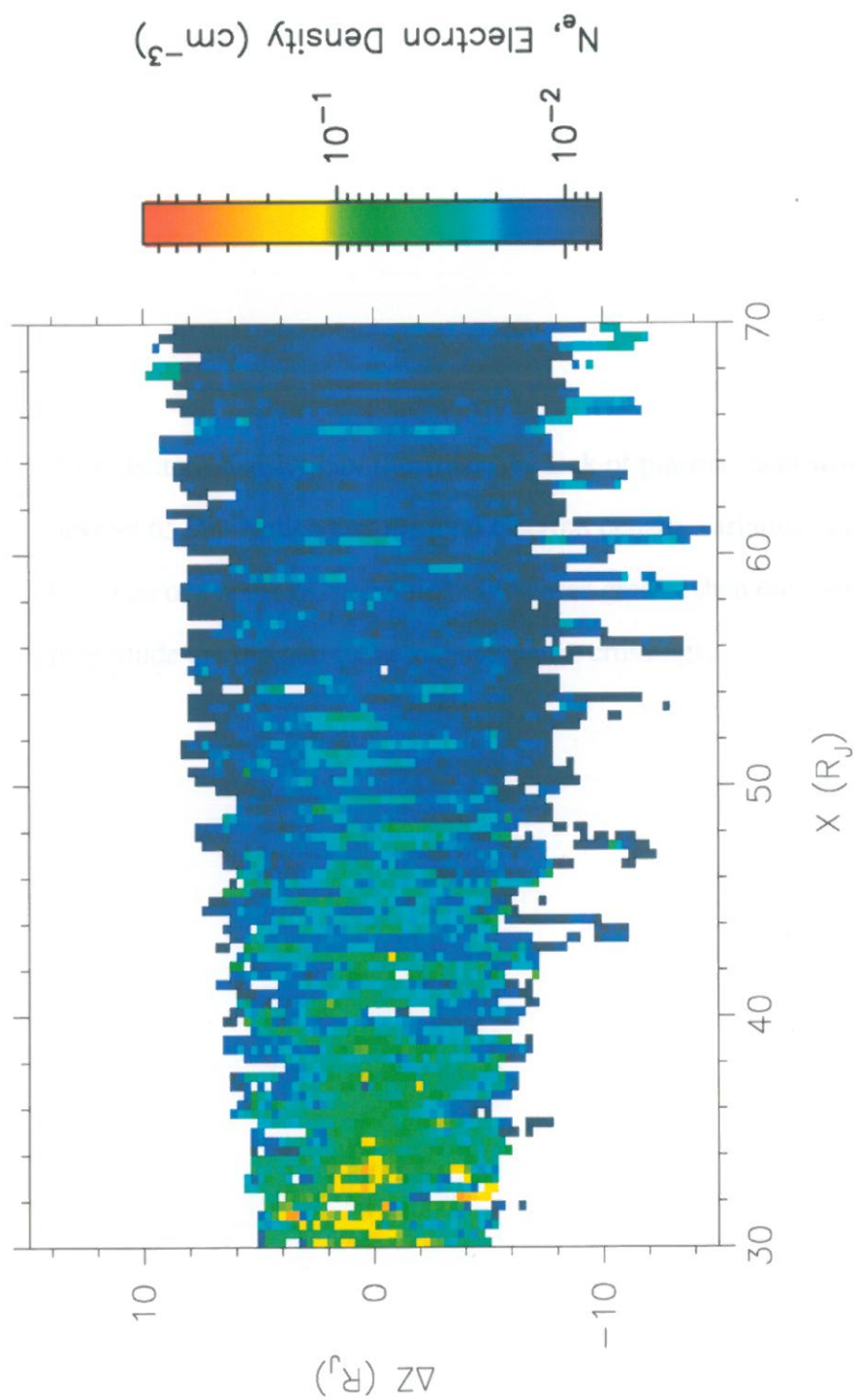1996 144 (May 23) 00:00:00 – 2002 308 (November 4) 00:00:00

Figure A.13   This electron density plot illustrates the lack of plasma sheet structure

beyond 65 R_J. Notice that the total electron density variation is limited to

less than one order of magnitude. Increases greater than one order of

magnitude are thought to be magnetopause crossings.

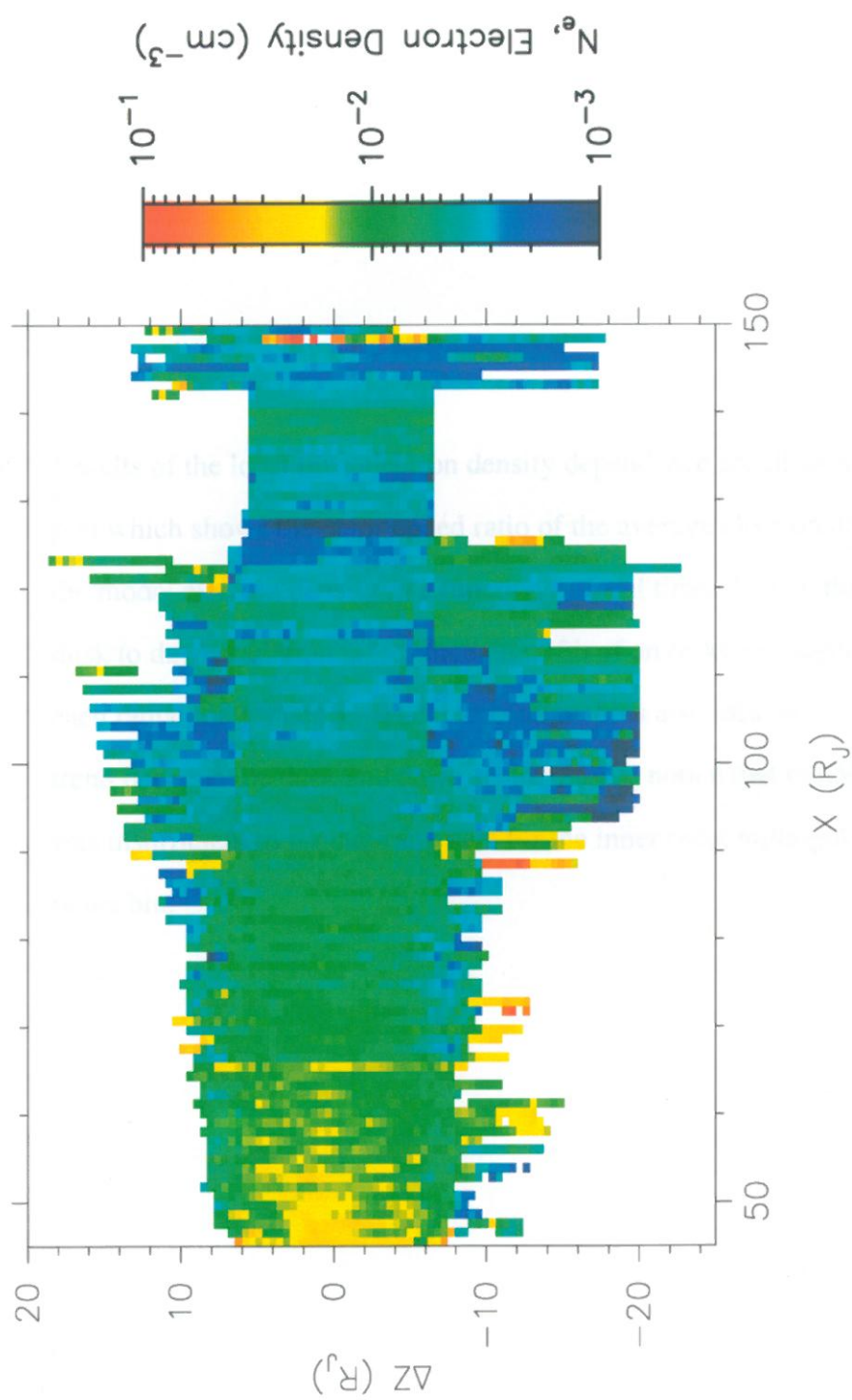1996 144 (May 23) 00:00:00 – 2002 308 (November 4) 00:00:00

Figure A.14   Results of the local time electron density dependence are illustrated in this

plot which shows the color coded ratio of the average electron density to

the model electron density as a function of local time. Notice that the total

dusk to dawn variation is less than one fifth of an order of magnitude for

each radial bin sequence. The intermediate bins also lack any consistent

trend between the dusk and dawn sectors. Also notice that radial coverage

was insufficient to produce any data for the inner most midnight to 0300

hours bin.

1996 175 (June 23) 00:00:00 − 2002 308 (November 4) 00:00:00
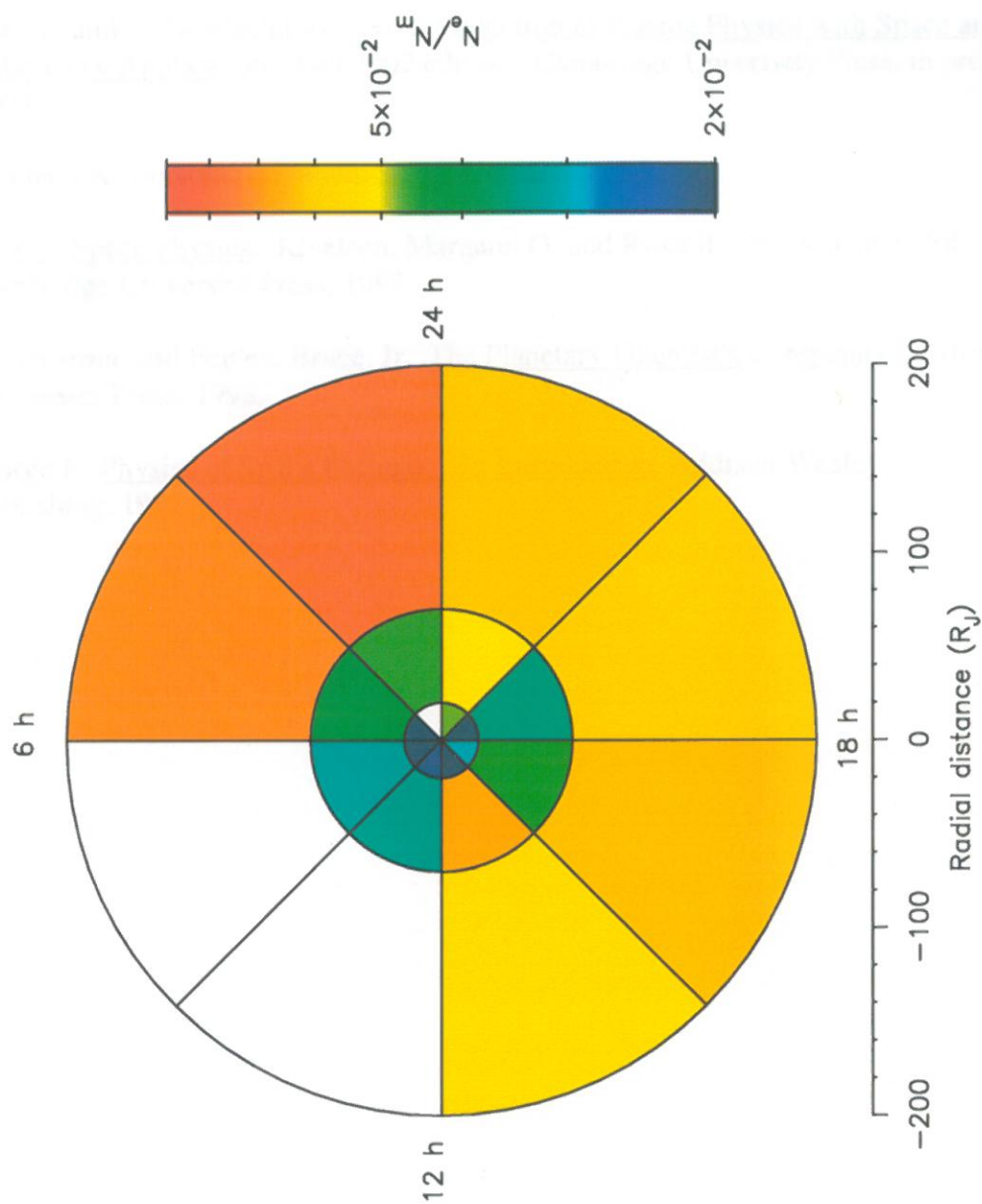
REFERENCES

Ansher, Jay Alan. <u>Electron Density at Jupiter Using the Galileo Plasma Wave Instrument</u>. Ph.D. thesis, University of Iowa, December 2001.

Gurnett, D. A., and A. Bhattacharjee. An <u>Introduction to Plasma Physics with Space and Laboratory Applications</u>, Fall 2002 edition. Cambridge University Press, in press, 2004.

Gurnett, Donald A. personal communication, University of Iowa.

<u>Introduction to Space Physics</u>. Kivelson, Margaret G. and Russell, Christopher T. Ed. Cambridge University Press, 1997.

Lodders, Katharina, and Fegley, Bruce, Jr. <u>The Planetary Scientist's Companion.</u> Oxford University Press, 1998.

Parks, George K. <u>Physics of Space Plasmas: An Introduction.</u> Addison Wesley Publishing, 1991.